Geophysical Research Letters

RESEARCH LETTER
10.1029/2023GL104497

Key Points:

- Largest database of land subsidence rates was compiled
- First global map of land subsidence rates was produced
- Comprehensive zonal statistics were calculated

Supporting Information:

Supporting Information may be found in the online version of this article.

Correspondence to:

P. Tahmasebi,
tahmasebi.pejman@gmail.com

Citation:

Davydzenka, T., Tahmasebi, P., & Shokri, N. (2024). Unveiling the global extent of land subsidence: The sinking crisis. *Geophysical Research Letters*, *51*, e2023GL104497. https://doi.org/10.1029/2023GL104497

Received 11 MAY 2023
Accepted 19 NOV 2023

Author Contributions:

Conceptualization: Pejman Tahmasebi
Data curation: Tsimur Davydzenka
Funding acquisition: Pejman Tahmasebi
Investigation: Tsimur Davydzenka
Resources: Pejman Tahmasebi
Software: Tsimur Davydzenka
Supervision: Pejman Tahmasebi
Validation: Tsimur Davydzenka, Nima Shokri
Visualization: Tsimur Davydzenka
Writing – original draft: Tsimur Davydzenka
Writing – review & editing: Pejman Tahmasebi, Nima Shokri

Unveiling the Global Extent of Land Subsidence: The Sinking Crisis

Tsimur Davydzenka[1], Pejman Tahmasebi[1], and Nima Shokri[2]

[1]Colorado School of Mines, Golden, CO, USA, [2]Institute of Geo-Hydroinformatics, Hamburg University of Technology, Hamburg, Germany

Abstract Land subsidence, referring to the vertical sinking of land surface, is a significant geohazard posing serious risks to security of infrastructure, natural resources, built environment, and businesses in numerous places worldwide. Using deep learning approaches combined with more than 46,000 subsidence data, we predicted global land subsidence based on 23 environmental parameters. The generated global map of land subsidence covers historically documented and new subsiding areas. We estimate that more than 6.3 million square kilometers of the global land is influenced by significant subsidence rates. That includes 231,000 square kilometers of urban and dense settlement areas and a population of nearly 2 billion. The model revealed a positive correlation between the intensity of groundwater abstraction and the subsidence rate. Our results offer new insights regarding potential hotspots of land subsidence and provide the information required to devise necessary action plans and develop effective policies to mitigate this growing challenge worldwide.

Plain Language Summary Land subsidence is a destructive phenomenon occurring around the globe causing damage to infrastructure, increased flood risks, and reduction of aquifer storage. However, prediction and quantification of land subsidence rates globally using physics-based methods presents a major challenge. Capitalizing on the robustness of modern deep learning methods and taking advantage of the increasingly available data sets of environmental parameters, this study introduces the first map of land subsidence rates on a global scale. The resulting map can be used for various geospatial modeling tasks, as well as to guide a more detailed local investigation of land subsidence.

1. Introduction

Land subsidence refers to gradual settlement or rapid sinking of the ground that can occur as a result of natural factors (e.g., volcanic or seismic activity, collapse of subsurface cavities, compaction of loose fine-grained deposits) or anthropogenic activities (e.g., excessive groundwater (GW) abstraction, mining, subsurface energy extraction) (Galloway & Burbey, 2011). Land subsidence can cause damage to infrastructure and lead to increased flood risks, and permanent reduction in aquifers' storage capacity. It can also cause disturbance to water management and possible repercussions such as increased saltwater intrusion as a result of reduction in land elevation and changes in the gradient of streams and drains. High maintenance costs for roads, railways, pipelines, and buildings are only a few examples of stresses brought upon by land subsidence. Although it is a gradual process, taking years to decades to develop, land subsidence presents serious socioeconomic, environmental and security challenges globally (Gambolati & Teatini, 2015; Xu et al., 2012).

Although land subsidence has been historically observed in low deltaic areas or coastal regions (Huang et al., 2012; Schmidt, 2015), it is being increasingly observed in large inland areas near densely urban, agricultural and industrial areas with high groundwater demand (Bonì et al., 2015; Gambolati & Teatini, 2015; Poland, 1987; Tomás et al., 2005). Excess groundwater extraction is believed to be one of the main causes of large-scale and high-magnitude land subsidence (Motagh et al., 2008; Poland & Davis, 1969; Sun et al., 1999). Groundwater over exploitation compacts the underground reservoirs because water is the element partly responsible for holding up the ground. The excess water withdrawal leads to compaction of the underlying depleted porous formation thus inducing land subsidence. The increase in the frequency and intensity of drought and the ever-growing demand for water almost by all sectors pose additional pressures on already stressed groundwater resources in many places, exacerbating the risks and vulnerability to land subsidence.

The total global extent of land surface susceptible to subsidence has been estimated to be 12 million km^2 (Herrera-García et al., 2021). Land subsidence has been observed all around the world, with major sites in

USA (Chen et al., 2016), China (Wang et al., 2009), Iran (Motagh et al., 2008), Indonesia (Abidin et al., 2013), Taiwan (Hung et al., 2018), Vietnam (Le et al., 2016), Egypt (Zaid et al., 2014), Japan (Sato et al., 2003), Mexico (Chaussard et al., 2014; Cigna & Tapete, 2022), and Italy (Bozzano et al., 2015) at rates as high as 430 mm/year. With the risks associated with land subsidence and the irreversible nature of some of its consequences, it is crucial to be able to accurately model its extent and rates. Even more so, since measuring it directly with the available methods such as global positioning system (GPS) or Interferometric Synthetic Aperture Radar (InSAR) on global scale is mostly prohibitive and presents its own set of complications (Smith & Majumdar, 2020; Wu et al., 2022). Furthermore, estimating subsidence requires integration of numerous variables and taking their respective impacts into account. To help identify areas that are susceptible to subsidence or in a few cases quantifying the rates, several research groups have applied machine learning methods based on the available local measurements of land subsidence and geospatial parameters. These methods have been applied to model subsidence in areas of Iran (Mohammady et al., 2019; Rahmati et al., 2019), UAE (Elmahdy et al., 2022), Greece (Ilia et al., 2018), South Korea (Bui et al., 2018), China (Zhou et al., 2019), Indonesia (Hakim et al., 2020), and USA (Smith & Majumdar, 2020) using relevant predictor maps that describe climate, topography, geology, soil properties, and hydrology of the study area.

Motivated by the importance of land subsidence and its effect on water management, disaster risks, urban planning and security of infrastructure, as well as a wide range of environmental factors, the specific objective of this study was to quantify and map land subsidence globally with a high spatial resolution. By conducting a systematic review of the subsidence literature and open-source records, we compiled what is, to our knowledge, the most extensive data set of subsidence rates. Using the data set and 23 spatially continuous environmental parameters, we trained a machine learning model, that learned to accurately predict subsidence at any location based on the provided predictors. We applied the resulting model to produce the first global map of subsidence rate to date, which can be used to identify previously undocumented subsiding areas, motivate further local investigation, and provide crucial information for developing actionable policies to manage and mitigate subsidence effects in vulnerable regions.

2. Data and Methods

In this section, we will discuss the steps that were followed to build the predictive model for quantifying rates of subsidence on a global scale. The entire methodology can be divided into three parts: 1-Preparation of global subsidence data set, 2-Selection of input variables, 3-Training the model. We direct the reader to Supporting Information S1, where we discuss the first two parts of the methodology, as well as calculation of zonal statistics.

Depending on the complexity of the model, any Artificial Neural Network (ANN) requires sufficient training data to achieve adequate accuracy. Therefore, it is essential to have sufficient amount of subsidence data (target parameter) for model training. Moreover, the target parameter in each location must be correlated with a comprehensive set of climatic, topographic, geological, hydrological, anthropological parameters (predictors) that can influence subsidence rates. Compiling and processing the spatial predictors are essential steps for training the model and is followed by establishing relationships between the predictors and the target parameter (land subsidence) through ANN. After validation of the trained model and assessment of its performance, the model can be applied to predict global subsidence rates and calculate zonal statistics.

We use Artificial Neural Networks (ANN) to produce the global subsidence map. To optimize network architecture (number of layers and neurons), we use a trial-and-error approach and iteratively adjusts hyperparameters by testing multiple layer/neuron combinations. Then, the most optimal model with its specifications is derived and used for the final computation. In this study, the final network architecture consisted of 3 hidden layers (512, 192, and 32 neurons), where each hidden layer was followed by a dropout layer (0.075, 0.15, 0.35 drop ratio). Based on the further sensitivity analysis, we found that the best model performance (highest R^2 score) was achieved by using the ELU activation functions and MSE loss function. This resulted in a model with an average correlation of $R = 0.82$. The data sets of subsidence records and predictors were assembled into 69,230 rows and 24 columns array, where each subsidence rate value (24st column) had 23 corresponding input values derived from predictor maps (25% of the rows represent 0-subsidence scenarios). Next, all continuous variables were transformed with StandardScaler—QuantileTransformer—MinMaxScaler pipeline (scikit-learn), and all categorical variables (Land Cover and Lithology) were transformed using One-Hot Encoder. The complete set was randomly split into training/validation/testing sets in 81/9/10 ratio and training was conducted for 960 epochs. A detailed description

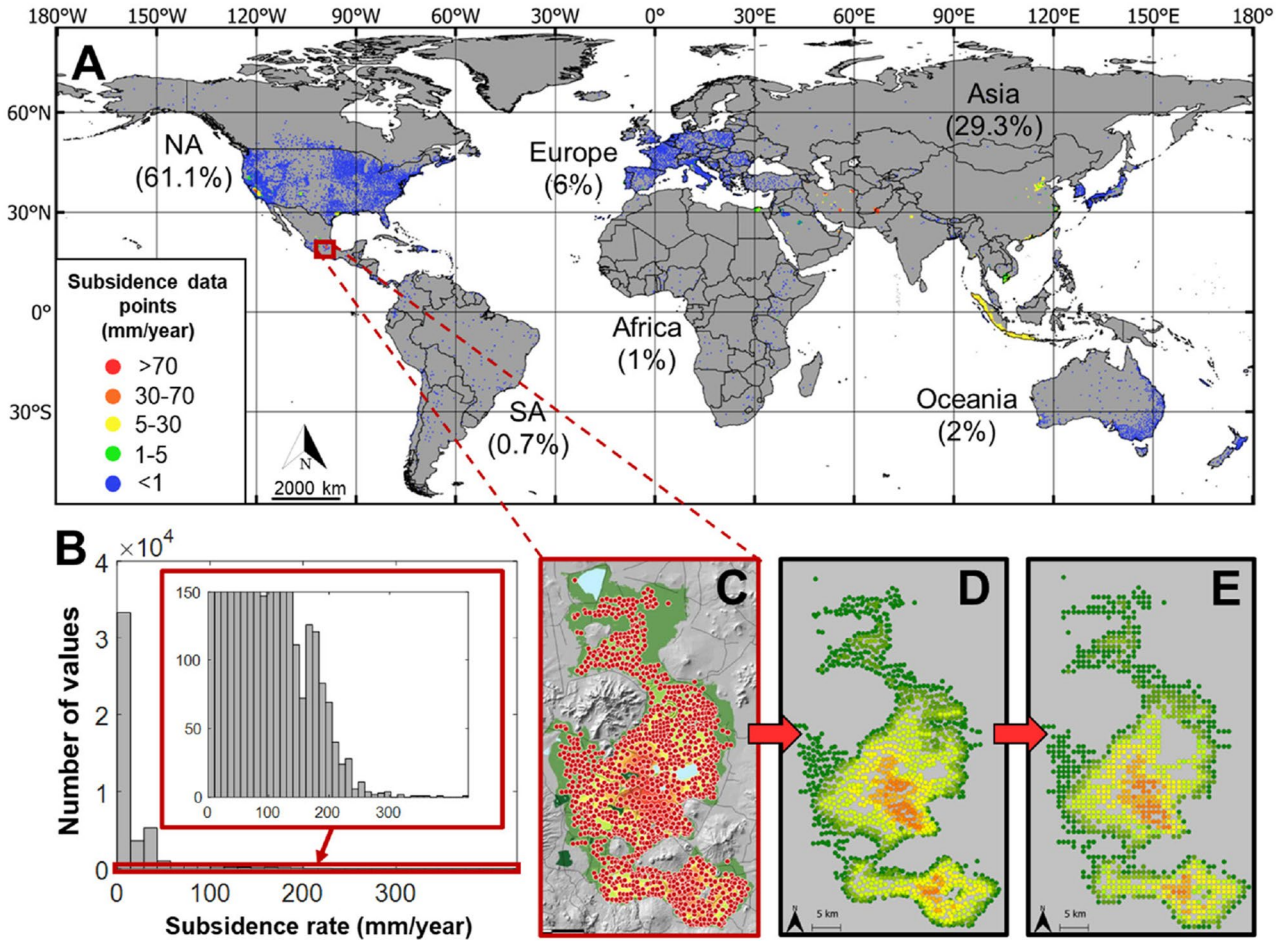

Figure 1. (a)—Locations of recorded subsidence rates. Includes 34 sources with reported subsidence maps that were subsequently digitized and converted to points at 30″ resolution, 193 sources with a single subsidence point per source, and 19221 GPS stations. (b)—Frequency distribution of the subsidence rates. (c–e)—Digitization workflow. (c)—Points detected by the digitization algorithm, based on the provided colors in the legend of the original image in Figure S1 of the Supporting Information S1. (d)—Visualization of the extracted points in GIS software, based on extracted longitude, latitude, and rates. (e)—Final locations of the points, after resampling and snapping on the 30″ tiles of the predictor maps.

of hyperparameters can be found in Figure S5 of the Supporting Information S1, and parity plots for training and testing data sets, for visualization of the model's accuracy.

3. Results and Discussions

3.1. Global Scale Prediction of Land Subsidence

We compiled subsidence data from 221 sources (see Table S1 in Supporting Information S1 for relevant information), which included digitized data from studies on land subsidence, as well as available remote sensing data. The total data set consisted of 253,882 data points, which after upsampling and averaging into a resolution of single point per 30″ (Figure 1) and removing unsubstantial rates (at ≤0 mm/y cutoff), as well as declustering all of the local studies resulted in more than 46,000 data points, to be later used in developing the predictive models.

We selected a comprehensive set of climatic, geological, and topographic parameters, and expanded the total number of predictors to 23 which were used for model training (Table S2 in Supporting Information S1). Utilizing machine learning approaches provides a valuable opportunity to determine the optimal size of the input vector to fully capture the effects of a wide range of parameters on land subsidence. Furthermore, these approaches mitigate the risk of overfitting, allowing the model to discern the key governing parameters. As subsidence is believed to be strongly linked to groundwater withdrawal and subsequent lowering of hydraulic head (Bagheri-Gavkosh

et al., 2021), we selected two variables that are proxies for groundwater abstraction and four variables for groundwater recharge, which, hypothetically, should enable the network to learn aquifer balance based on the data in the training set. Next, as it was argued that climatic conditions are an important predictor of subsidence (Andaryani et al., 2019; Carbognin & Tosi, 2002; Galloway et al., 2016; Shirzaei & Bürgmann, 2018), we selected nine continuous climate variables, which describe temperatures, precipitation, vegetation, etc. at any given location. For geology, we selected more six features that characterize soil properties and composition, sediment thickness, and groundwater storage capacity. Lastly, among the topography descriptors, we selected two variables namely slope and topographic wetness index, which are widely used in environmental modeling.

The final predictive model was created based on the aggregated data set. From the preliminary analysis, we found that an architecture with three hidden layers and 740 total neurons resulted in the most optimal performance (full specifications are listed in Figure S5 of the Supporting Information S1). After evaluating network performance on the test data set (10% of the data, randomly selected prior to training while maintaining the equivalent distribution of high and low rates of subsidence) we were able to confirm the model's reasonable prediction accuracy. Despite the prevalence of low rates in the data set, the model performs well in the entirety of the subsidence range (0–430 mm/y), as evidenced by the scatter plot displayed in Figure S6 of the Supporting Information S1. The global map produced by the model is provided in Figure 2a. More detailed visualizations at the continental and regional levels are shown in Figures 2b–2d and Figures S8–S14 in Supporting Information S1.

3.2. Feature Importance and Validation

One of the limitations of ANNs is its black box nature, which leads to model interpretability challenges. In this study, model interpretation is conducted by taking advantage the state-of-the-art method in model interpretability—SHAP (Lundberg & Lee, 2017), which we apply to assess the importance of the predictors in modeling land subsidence rate. Moreover, in addition to calculating importance as a relative score, we quantify whether a predictor has a positive, negative, or mixed (conditional) impact on subsidence (see Supporting Information S1 for details). A positive impact indicates that an increase in the predictor value leads to an increase in the subsidence rate, while negative impact means that increase in the predictor value leads to a decrease in the subsidence rate. A mixed impact is classified as a feature-subsidence relationship where, depending on the values of other conditions, a high value of a predictor will lead to an increase or decrease in the subsidence rate.

Among the 23 input features, we found that all groundwater extraction proxies have a positive impact on land subsidence rates, which agrees with the observations and previous studies (Galloway & Burbey, 2011; Xu et al., 2008). Moreover, GW abstraction was found to be the main predictor of subsidence, outperforming the second-best predictor by 62% in terms of overall importance (see Figure 3, Figure S7, and Table S4 in Supporting Information S1 for more details). The second most influential parameter was found to be seismic hazard, measured in peak ground acceleration. Next, we found that environmental parameters that directly or indirectly affect aquifer or groundwater recharge have an expected negative impact on subsidence, which is valid for climatic (precipitation of wettest quarter and annual precipitation) and hydrological (groundwater recharge) parameters. Next, potential subsidence magnitude is controlled by the thickness of the sedimentary layer, where the larger values generally mean more available pore space for compaction (Smith & Majumdar, 2020). The results of the feature importance analysis indicate that the main proxy for sedimentary thickness (average soil and sedimentary deposit thickness) as well as water storage thickness exhibit positive impact on subsidence. However, water storage thickness has demonstrated conditional impacts on subsidence rate, which is supported by the fact that most of the largest aquifers in the world are not susceptible to compaction compared to small aquifers (Richts & Vrba, 2016). Next, among all temperature-related variables, only mean temperature of warmest quarter was found to have a non-trivial and non-conditional impact on subsidence. The high values of this predictor correlate with arid and semi-arid regions, which is where the majority of subsidence is observed (Bagheri-Gavkosh et al., 2021; Herrera-García et al., 2021). Contrary to the hypothesis that evapotranspiration promotes subsidence (Smith & Majumdar, 2020), it was found to have a negative effect on the rate. While the proposition may be true at a local level, the highest global evapotranspiration values correspond to areas with rich vegetation, which are generally not susceptible or correlated with high rates of land subsidence. We should also note that any single variable has only a limited effect on the final prediction, and although the elevation has a positive effect on the final output, the model produces the output based on all available features. Soil descriptors such as clay content was identified as having a positive impact on the subsidence rates, which is supported by the fact that presence of clays in the

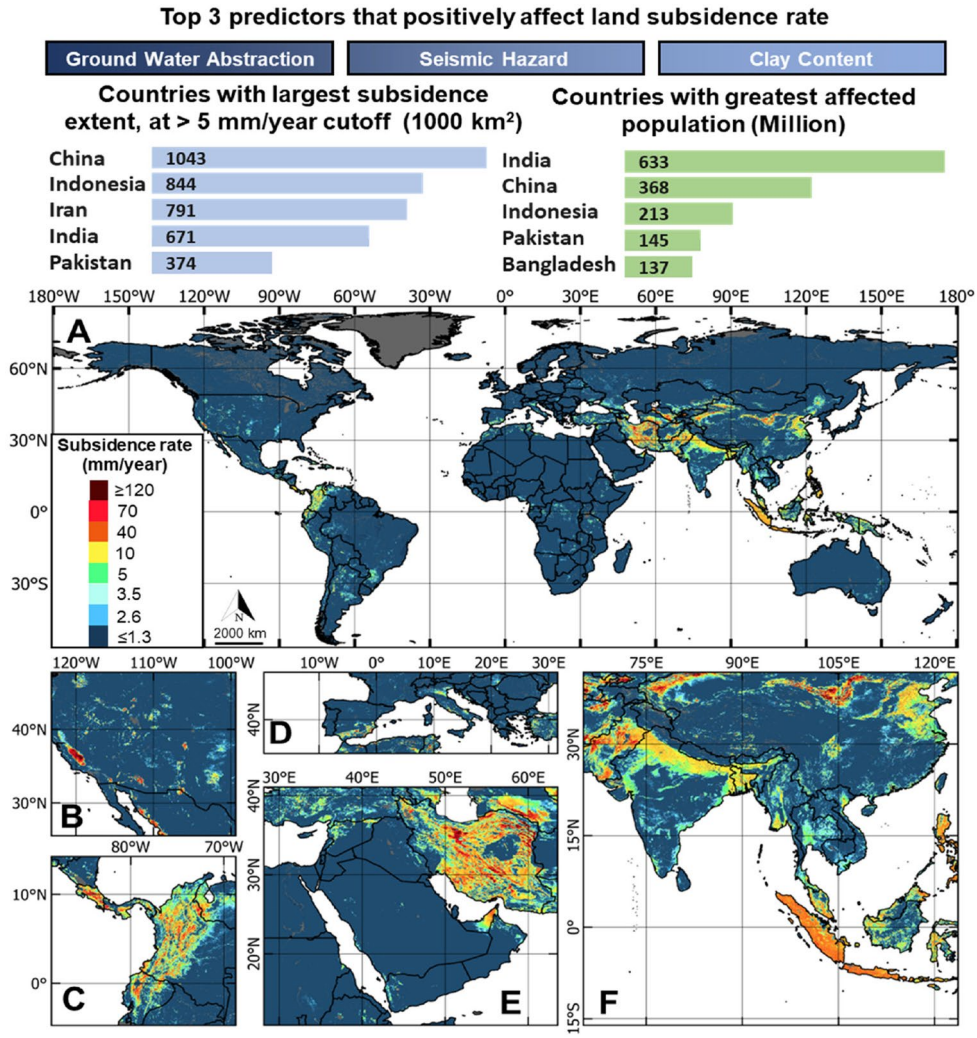

Figure 2. Global prediction of land subsidence, with relevant feature importance and zonal statistics at the top of the figure. Modeled subsidence rates for the entire globe (a), zoomed-in maps of land subsidence for North America (b), South America (c), Europe and North Africa (d), Middle East (e), and South, East, and South-East Asia (f). The zoomed in maps were visualized with unique color scales that are different from the global map (a) and are included in Supporting Information S1 with additional maps of land subsidence at global, continental, and regional level in Figures S8–S14 of the Supporting Information S1. The model was trained using the subsidence data points presented in Figure 1 and a comprehensive set of environmental parameters listed in Table S2 of the Supporting Information S1. Gaussian smoothing has been applied to enhance the visualization (including Figures S8–S14 in Supporting Information S1).

aquifer reduces its resistance to subsidence, because of their weak geomechanical properties. However, the measurements of soil content were only conducted for the top 200 cm layer, which is not entirely representative of the actual aquifer composition. Organic carbon density was found to have a negative impact on the subsidence rates, which could be the subject of future research. Lastly, the impact of population is consistent with the observations that subsidence generally occurs in densely populated areas which puts a strain on associated aquifers. The rest of the variables were found to have either conditional or not easily classifiable impact (generally features with the least overall importance).

3.3. Implications: Affected Areas, Population, and Infrastructure

Using relevant global data sets (see Supporting Information S1 for details), we calculated the total affected population in subsiding areas in 2020 and the magnitude of subsidence rates in urban and dense settlement areas with four different thresholds. The corresponding maps of the affected population at >5 mm/y threshold are displayed

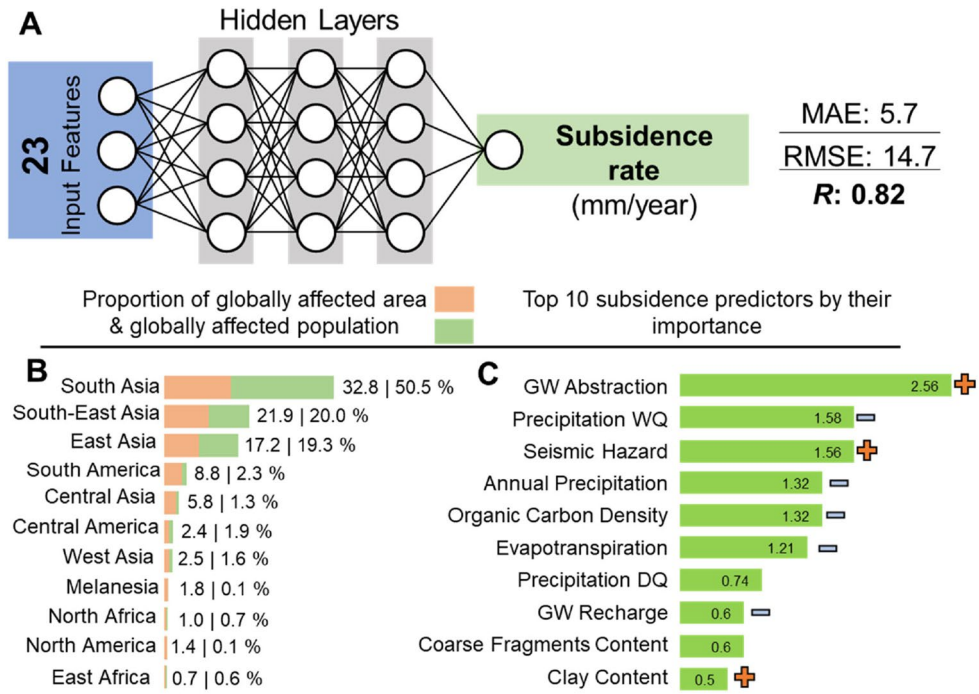

Figure 3. Summary of the methodology and results. Simplified architecture of utilized machine learning model (a), proportions of land area and population affected worldwide by land subsidence larger than 5 mm/year by region (b), and importance and impact of the predictors (c).

in Figures S15a–S15f of the Supporting Information S1, and maps of regions with the greatest affected urban and dense settlement extent are shown in Figures S15g–S15i of the Supporting Information S1. The extent to which subsidence can affect population can be expressed as damages to infrastructure, increased flood risks, and permanent storage reduction in aquifer systems (Dinar et al., 2021). We estimate that a cumulative area of over 6.3 million km^2 worldwide is subsiding at rates higher than 5 mm/y (~5% of total global land area). That comprises 231,000 km^2 of urban and dense settlement areas, as well as approximately 2 billion people that live in the immediate subsiding areas. By classifying the world into different zones based on lithology, land cover, climate, biomes, anthropogenic biomes, regions, and countries (Table S4 in Supporting Information S1), we calculated the following relevant zonal statistics (Tables S5 and S6 in Supporting Information S1). Unconsolidated sediments at all thresholds comprise the largest total subsidence extent which, at >5 mm/y cutoff, accounts for nearly 3.8 Mkm^2 (59% of all subsidence area at that threshold) and constitutes ~10% of unconsolidated sediments worldwide. The highest maximum rates at 320.6 mm/y was also predicted for this lithological class. Next, in terms of land cover, we found that cultivated and managed areas comprise the largest total subsidence extent of nearly 2.1 Mkm^2 (12.2% of the global class area, at >5 mm/y cutoff). The subtropical highland or temperate oceanic climate was found to have the largest maximum subsidence rates, while the tropical rainforest climate is characterized by the largest subsidence extent. At the highest threshold (>50 mm/y) we found that on the regional level, South Asia accounts for the largest subsidence extent worldwide (2.2% of its total area is affected by >50 mm/year subsidence) as well as for the largest affected population (20 mln. people). Among the 195 countries considered for zonal analysis, the top five countries with the largest mean subsidence rates were found to be Philippines, Iran, Costa Rica, Indonesia, Uzbekistan, while the top five countries by the subsidence extent (>5 mm/y) were Indonesia, China, Indonesia, Iran, India, and Pakistan. Lastly, at the highest threshold, Mexico accounts for the highest predicted subsidence of 320.5 mm/y. For complete zonal analysis, we direct the reader to Supporting Information S1.

4. Conclusions

In this study, we developed a predictive model to quantify the subsidence rate on a global scale, which enabled us to produce the first global map of subsidence rates. The analysis of the feature impact and importance allowed us

to further validate the model and potentially observe undiscovered relationships between environmental parameters and subsidence. The demonstrated importance and positive correlation of groundwater withdrawal proxies and subsidence magnitudes agrees with the previously observed dominant effect of these parameters. While our model has been validated by a reasonable correlation coefficient score, as well as feature importance and zonal statistics analysis that are consistent with the literature, it can be further improved. As it is invariably the product of the richness of the training data and quality of the predictors, enhancements can be made when more subsidence data and higher precision predictor data sets become available. Another significant aspect is data imbalance. Approximately half of the data set indicates very small subsidence, which could affect the model's performance for minority classes. Although this is typical for Earth science data, further research is still required. Additionally, the data set may suffer from spatial and temporal autocorrelation as the existing data, due to local financial and geopolitical limitations, are compiled predominantly from only a few subsidence hotspots around the world, leading to data clustering which can cause bias in spatial statistics when the sampling locations are not evenly distributed. Another major source of uncertainty is variable spatial rates, where some subsidence sites are represented by thousands of data points, while in other sites only a single data point is available. As such, areas with denser data coverage tend to have a more significant influence on spatial predictions. This clustering could inflate the evaluations metrics due to the possible presence of digitized data in both training and test data sets. For a similar reason, the reliability of the model can also differ at the continent level, since continents such as South America, Africa, and Australia are significantly underrepresented in terms of reported subsidence data. Due to computational burden associated with conducting environmental studies on a global scale, this methodology does not account for the spatial relationships between input points. Which means that, hypothetically, a point with no groundwater abstraction surrounded by points with high groundwater abstraction may realistically experience subsidence, however the model would not be able to capture it, since surrounding points are not taken into consideration when it makes a prediction. Though, accounting for the spatial relationships between surrounding points is something that the authors considered in the past for regional studies (Bai & Tahmasebi, 2023). The model also does not incorporate information about the depth of groundwater abstraction, aquifer type, or oil and gas production, all of which are important predictors of land subsidence. Potential multicollinearity among some of the input features (although ANNs are generally robust to it) is another direction that can be considered for future studies. From the perspective of model architecture, as is the case with other ML models, more advanced algorithms can be utilized to optimize its parameters. Finally, as land subsidence is a dynamic process, that is often observed with a considerable time lag to groundwater table decline, the greatest accuracy improvements will be achieved once detailed temporal data sets of groundwater abstraction or its proxies are introduced. If future projections of such data become available, it could enable modeling of future land subsidence rates and consequently total sediment compaction.

As of now, the presented subsidence maps should be used to guide further investigation of the areas that were recognized by the model to have significant subsidence rates (e.g., in South Asia, Central America, northern parts of South America, and other regions). Only direct subsidence measurements can definitively quantify effective rates, especially in urban areas that are subject to small-scale variations and around aquifers that are characterized by small-scale (<1 km) heterogeneities. Our assessment shows that 5% of the global area and 25% of the population are affected by significant land subsidence. These numbers are expected to rise, as changing climate, increasingly prolonged periods of drought, and growing population only exacerbate global dependency on groundwater. As such, these maps can be used to increase awareness, help plan mitigation measures, and provide a foundation for optimized and regulated groundwater use policy. Additionally, the maps will be useful for such practical applications as urban planning and infrastructure development for cities that are located in subsiding areas. Furthermore, knowledge of land subsidence rates will be instrumental for the insurance purposes as areas with high subsidence rates could be more susceptible to potential hazards. Finally, as subsidence can affect water drainage, leading to waterlogging or altered flow patterns, the map can be used by farmers and land managers to adapt their irrigation practices and crop choices.

The significance of our analysis lies in its ability to provide a wide range of actors including policymakers, farmers and landowners, urban planners, and natural disaster managers with required analytics and information to understand the global extent of land subsidence. This study also provides valuable data for devising the necessary action plans and targeted interventions to mitigate or minimize the adverse impacts of land subsidence on human population, infrastructure, ecosystem, and businesses thus contributing to several United Nations Sustainable Development Goals (UN SDGs) particularly SDG 9, 10, 11, and 15. Moreover, the resulting global subsidence

map can be integrated with other global scale studies. For instance, it can be used with global climate models to provide a holistic view of vulnerabilities to sea-level rise (e.g., for a coastal city facing both sea-level rise and significant land subsidence, the combined risk could be greater than previously estimated). Additionally, the study can be combined with global water scarcity reports to formulate comprehensive water management policies (areas with both high subsidence rates and water scarcity could be prioritized for immediate intervention). Finally, merging the finding with global economic data can help governments and agencies in evaluating the economic impact of land subsidence to prioritize their funding and intervention programs.

Conflict of Interest

The authors declare no conflicts of interest relevant to this study.

Data Availability Statement

References to all data that was used in this study are compiled in Supporting Information S1 (Table S1, S2, and S4). Data Sets S1–S3 are available at Zenodo public repository (Davydzenka et al., 2023, https://doi.org/10.5281/zenodo.10223637).

Acknowledgments
We acknowledge all data providers, without whom this work would not be possible.

References

Abidin, H. Z., Gumilar, I., Andreas, H., Murdohardono, D., & Fukuda, Y. (2013). On causes and impacts of land subsidence in Bandung Basin, Indonesia. *Environmental Earth Sciences*, *68*(6), 1545–1553. https://doi.org/10.1007/s12665-012-1848-z

Andaryani, S., Nourani, V., Trolle, D., Dehgani, M., & Asl, A. M. (2019). Assessment of land use and climate change effects on land subsidence using a hydrological model and radar technique. *Journal of Hydrology*, *578*, 124070. https://doi.org/10.1016/j.jhydrol.2019.124070

Bagheri-Gavkosh, M., Hosseini, S. M., Ataie-Ashtiani, B., Sohani, Y., Ebrahimian, H., Morovat, F., & Ashrafi, S. (2021). Land subsidence: A global challenge. *Science of the Total Environment*, *778*, 146193. https://doi.org/10.1016/j.scitotenv.2021.146193

Bai, T., & Tahmasebi, P. (2023). Graph neural network for groundwater level forecasting. *Journal of Hydrology*, *616*, 128792. https://doi.org/10.1016/J.JHYDROL.2022.128792

Bonì, R., Herrera, G., Meisina, C., Notti, D., Béjar-Pizarro, M., Zucca, F., et al. (2015). Twenty-year advanced DInSAR analysis of severe land subsidence: The Alto Guadalentín Basin (Spain) case study. *Engineering Geology*, *198*, 40–52. https://doi.org/10.1016/j.enggeo.2015.08.014

Bozzano, F., Esposito, C., Franchi, S., Mazzanti, P., Perissin, D., Rocca, A., & Romano, E. (2015). Understanding the subsidence process of a quaternary plain by combining geological and hydrogeological modelling with satellite InSAR data: The Acque Albule Plain case study. *Remote Sensing of Environment*, *168*, 219–238. https://doi.org/10.1016/j.rse.2015.07.010

Bui, D. T., Shahabi, H., Shirzadi, A., Chapi, K., Pradhan, B., Chen, W., et al. (2018). Land subsidence susceptibility mapping in South Korea using machine learning algorithms. *Sensors*, *18*(8), 2464. https://doi.org/10.3390/s18082464

Carbognin, L., & Tosi, L. (2002). Interaction between climate changes, eustacy and land subsidence in the North Adriatic Region, Italy. *Marine Ecology*, *23*(1), 38–50. https://doi.org/10.1111/j.1439-0485.2002.tb00006.x

Chaussard, E., Wdowinski, S., Cabral-Cano, E., & Amelung, F. (2014). Land subsidence in central Mexico detected by ALOS InSAR time-series. *Remote Sensing of Environment*, *140*, 94–106. https://doi.org/10.1016/j.rse.2013.08.038

Chen, J., Knight, R., Zebker, H. A., & Schreüder, W. A. (2016). Confined aquifer head measurements and storage properties in the San Luis Valley, Colorado, from spaceborne InSAR observations. *Water Resources Research*, *52*(5), 3623–3636. https://doi.org/10.1002/2015WR018466

Cigna, F., & Tapete, D. (2022). Urban growth and land subsidence: Multi-decadal investigation using human settlement data and satellite InSAR in Morelia, Mexico. *Science of the Total Environment*, *811*. https://doi.org/10.1016/j.scitotenv.2021.152211

Davydzenka, T., Tahmasebi, P., & Shokri, N. (2023). Data for "unveiling the global extent of land subsidence: The sinking crisis" [Dataset]. Zenodo. https://doi.org/10.5281/zenodo.10223637

Dinar, A., Esteban, E., Calvo, E., Herrera, G., Teatini, P., Tomás, R., et al. (2021). We lose ground: Global assessment of land subsidence impact extent. *Science of the Total Environment*, *786*. https://doi.org/10.1016/j.scitotenv.2021.147415

Elmahdy, S. I., Mohamed, M. M., Ali, T. A., Abdalla, J. E. D., & Abouleish, M. (2022). Land subsidence and sinkholes susceptibility mapping and analysis using random forest and frequency ratio models in Al Ain, UAE. *Geocarto International*, *37*(1), 315–331. https://doi.org/10.1080/10106049.2020.1716398

Galloway, D. L., & Burbey, T. J. (2011). Review: Regional land subsidence accompanying groundwater extraction. *Hydrogeology Journal*, *19*(8), 1459–1486. https://doi.org/10.1007/s10040-011-0775-5

Galloway, D. L., Erkens, G., Kuniansky, E. L., & Rowland, J. C. (2016). Preface: Land subsidence processes. *Hydrogeology Journal*, *24*(3), 547–550. https://doi.org/10.1007/s10040-016-1386-y

Gambolati, G., & Teatini, P. (2015). Geomechanics of subsurface water withdrawal and injection. *Water Resources Research*, *51*(6), 3922–3955. https://doi.org/10.1002/2014WR016841

Hakim, W. L., Achmad, A. R., & Lee, C. W. (2020). Land subsidence susceptibility mapping in Jakarta using functional and meta-ensemble machine learning algorithm based on time-series InSAR data. *Remote Sensing*, *12*(21), 1–26. https://doi.org/10.3390/rs12213627

Herrera-García, G., Ezquerro, P., Tomas, R., Béjar-Pizarro, M., López-Vinielles, J., Rossi, M., et al. (2021). Mapping the global threat of land subsidence. *Science*, *371*(6524), 34–36. https://doi.org/10.1126/science.abb8549

Huang, B., Shu, L., & Yang, Y. S. (2012). Groundwater overexploitation causing land subsidence: Hazard risk assessment using field observation and spatial modelling. *Water Resources Management*, *26*(14), 4225–4239. https://doi.org/10.1007/s11269-012-0141-y

Hung, W. C., Hwang, C., Chen, Y. A., Zhang, L., Chen, K. H., Wei, S. H., et al. (2018). Land subsidence in Chiayi, Taiwan, from compaction well, leveling and ALOS/PALSAR: Aquaculture-induced relative sea level rise. *Remote Sensing*, *10*(1), 40. https://doi.org/10.3390/rs10010040

Ilia, I., Loupasakis, C., & Tsangaratos, P. (2018). Land subsidence phenomena investigated by spatiotemporal analysis of groundwater resources, remote sensing techniques, and random forest method: The case of Western Thessaly, Greece. *Environmental Monitoring and Assessment*, *190*(11), 623. https://doi.org/10.1007/s10661-018-6992-9

Le, T. S., Chang, C. P., Nguyen, X. T., & Yhokha, A. (2016). TerraSAR-X data for high-precision land subsidence monitoring: A case study in the historical centre of Hanoi, Vietnam. *Remote Sensing*, *8*(4), 338. https://doi.org/10.3390/rs8040338

Lundberg, S. M., & Lee, S. I. (2017). A unified approach to interpreting model predictions. In *Advances in neural information processing systems* (pp. 4766–4775).

Mohammady, M., Pourghasemi, H. R., & Amiri, M. (2019). Land subsidence susceptibility assessment using random forest machine learning algorithm. *Environmental Earth Sciences*, *78*(16), 503. https://doi.org/10.1007/s12665-019-8518-3

Motagh, M., Walter, T. R., Sharifi, M. A., Fielding, E., Schenk, A., Anderssohn, J., & Zschau, J. (2008). Land subsidence in Iran caused by widespread water reservoir overexploitation. *Geophysical Research Letters*, *35*(16), L16403. https://doi.org/10.1029/2008GL033814

Poland, J. F. (1987). Guidebook to studies of land subsidence due to ground-water withdrawal. *Tunnelling and Underground Space Technology*, *2*. https://doi.org/10.1016/0886-7798(87)90022-8

Poland, J. F., & Davis, G. H. (1969). Land subsidence due to withdrawal of fluids. *GSA Reviews in Engineering Geology*, *2*, 187–269. https://doi.org/10.1130/REG2-p187

Rahmati, O., Falah, F., Naghibi, S. A., Biggs, T., Soltani, M., Deo, R. C., et al. (2019). Land subsidence modelling using tree-based machine learning algorithms. *Science of the Total Environment*, *672*, 239–252. https://doi.org/10.1016/j.scitotenv.2019.03.496

Richts, A., & Vrba, J. (2016). Groundwater resources and hydroclimatic extremes: Mapping global groundwater vulnerability to floods and droughts. *Environmental Earth Sciences*, *75*(10), 926. https://doi.org/10.1007/s12665-016-5632-3

Sato, H. P., Abe, K., & Ootaki, O. (2003). GPS-measured land subsidence in Ojiya City, Niigata Prefecture, Japan. *Engineering Geology*, *67*(3–4), 379–390. https://doi.org/10.1016/S0013-7952(02)00221-1

Schmidt, C. (2015). Alarm over a sinking delta. *Science*, *348*(6237), 845–846. https://doi.org/10.1126/science.348.6237.845

Shirzaei, M., & Bürgmann, R. (2018). Global climate change and local land subsidence exacerbate inundation risk to the San Francisco Bay Area. *Science Advances*, *4*(3). https://doi.org/10.1126/sciadv.aap9234

Smith, R. G., & Majumdar, S. (2020). Groundwater storage loss associated with land subsidence in western United States mapped using machine learning. *Water Resources Research*, *56*(7), e2019WR026621. https://doi.org/10.1029/2019WR026621

Sun, H., Grandstaff, D., & Shagam, R. (1999). Land subsidence due to groundwater withdrawal: Potential damage of subsidence and sea level rise in southern New Jersey, USA. *Environmental Geology*, *37*(4), 290–296. https://doi.org/10.1007/s002540050386

Tomás, R., Márquez, Y., Lopez-Sanchez, J. M., Delgado, J., Blanco, P., Mallorquí, J. J., et al. (2005). Mapping ground subsidence induced by aquifer overexploitation using advanced Differential SAR Interferometry: Vega Media of the Segura River (SE Spain) case study. *Remote Sensing of Environment*, *98*(2–3), 269–283. https://doi.org/10.1016/j.rse.2005.08.003

Wang, G. Y., You, G., Shi, B., Yu, J., & Tuck, M. (2009). Long-term land subsidence and strata compression in Changzhou, China. *Engineering Geology*, *104*(1–2), 109–118. https://doi.org/10.1016/j.enggeo.2008.09.001

Wu, P. C., Wei, M., & D'Hondt, S. (2022). Subsidence in coastal cities throughout the world observed by InSAR. *Geophysical Research Letters*, *49*(7), e2022GL098477. https://doi.org/10.1029/2022GL098477

Xu, Y. S., Ma, L., Shen, S. L., & Sun, W. J. (2012). Evaluation of land subsidence by considering underground structures that penetrate the aquifers of Shanghai, China. *Hydrogeology Journal*, *20*(8), 1623–1634. https://doi.org/10.1007/s10040-012-0892-9

Xu, Y. S., Shen, S. L., Cai, Z. Y., & Zhou, G. Y. (2008). The state of land subsidence and prediction approaches due to groundwater withdrawal in China. *Natural Hazards*, *45*(1), 123–135. https://doi.org/10.1007/s11069-007-9168-4

Zaid, S. M., Mamoun, M. M., & Al-Mobark, N. M. (2014). Vulnerability assessment of the impact of sea level rise and land subsidence on North Nile Delta region. *World Applied Sciences Journal*. https://doi.org/10.5829/idosi.wasj.2014.32.03.14505

Zhou, C., Gong, H., Chen, B., Li, X., Li, J., Wang, X., et al. (2019). Quantifying the contribution of multiple factors to land subsidence in the Beijing Plain, China with machine learning technology. *Geomorphology*, *335*, 48–61. https://doi.org/10.1016/j.geomorph.2019.03.017

References From the Supporting Information

Abatzoglou, J. T., Dobrowski, S. Z., Parks, S. A., & Hegewisch, K. C. (2018). TerraClimate, a high-resolution global dataset of monthly climate and climatic water balance from 1958-2015. *Scientific Data*, *5*(1), 170191. https://doi.org/10.1038/sdata.2017.191

Abdollahi, S., Pourghasemi, H. R., Ghanbarian, G. A., & Safaeian, R. (2019). Prioritization of effective factors in the occurrence of land subsidence and its susceptibility mapping using an SVM model and their different kernel functions. *Bulletin of Engineering Geology and the Environment*, *78*(6), 4017–4034. https://doi.org/10.1007/s10064-018-1403-6

Arabameri, A., Chandra Pal, S., Rezaie, F., Chakrabortty, R., Chowdhuri, I., Blaschke, T., & Thi Ngo, P. T. (2021). Comparison of multi-criteria and artificial intelligence models for land-subsidence susceptibility zonation. *Journal of Environmental Management*, *284*, 112067. https://doi.org/10.1016/j.jenvman.2021.112067

Arabameri, A., Santosh, M., Rezaie, F., Saha, S., Coastache, R., Roy, J., et al. (2022). Application of novel ensemble models and k-fold CV approaches for Land subsidence susceptibility modelling. *Stochastic Environmental Research and Risk Assessment*, *36*(1), 201–223. https://doi.org/10.1007/s00477-021-02036-7

Auvinet, G., Méndez, E., & Juárez, M. (2017). Recent information on Mexico City subsidence. In *ICSMGE 2017—19th international conference on soil mechanics and geotechnical engineering* (pp. 3295–3298).

Azarakhsh, Z., Azadbakht, M., & Matkan, A. (2022). Estimation, modeling, and prediction of land subsidence using Sentinel-1 time series in Tehran-Shahriar plain: A machine learning-based investigation. *Remote Sensing Applications: Society and Environment*, *25*, 100691. https://doi.org/10.1016/j.rsase.2021.100691

Bekaert, D. P. S., Hamlington, B. D., Buzzanga, B., & Jones, C. E. (2017). Spaceborne synthetic aperture radar survey of subsidence in Hampton Roads, Virginia (USA). *Scientific Reports*, *7*(1), 14752. https://doi.org/10.1038/s41598-017-15309-5

Blewitt, G., Kreemer, C., Hammond, W. C., & Gazeaux, J. (2016). MIDAS robust trend estimator for accurate GPS station velocities without step detection. *Journal of Geophysical Research: Solid Earth*, *121*(3), 2054–2068. https://doi.org/10.1002/2015JB012552

Chaussard, E., Amelung, F., & Abidin, H. Z. (2012). Sinking cities in Indonesia: Space-geodetic evidence of the rates and spatial distribution of land subsidence. In *Proceedings of 'Fringe 2011 workshop', Frascati, Italy, 19–23 September 2011 (ESA SP-697, January 2012), 2011(September 2011), 19–23*. Retrieved from https://earth.esa.int/documents/10174/1573054/Sinking_cities_Indonesia_space-geodetic_evidence_rates_spatial_distribution_land_subsidence.pdf

Chen, M., Tomás, R., Li, Z., Motagh, M., Li, T., Hu, L., et al. (2016). Imaging land subsidence induced by groundwater extraction in Beijing (China) using satellite radar interferometry. *Remote Sensing*, *8*(6), 468. https://doi.org/10.3390/rs8060468

Chen, Q., Liu, G., Ding, X., Hu, J. C., Yuan, L., Zhong, P., & Omura, M. (2010). Tight integration of GPS observations and persistent scatterer InSAR for detecting vertical ground motion in Hong Kong. *International Journal of Applied Earth Observation and Geoinformation*, *12*(6), 477–486. https://doi.org/10.1016/j.jag.2010.05.002

Cigna, F., & Tapete, D. (2021). Present-day land subsidence rates, surface faulting hazard and risk in Mexico City with 2014–2020 Sentinel-1 IW InSAR. *Remote Sensing of Environment*, *253*, 112161. https://doi.org/10.1016/j.rse.2020.112161

Del Soldato, M., Farolfi, G., Rosi, A., Raspini, F., & Casagli, N. (2018). Subsidence evolution of the Firenze-Prato-Pistoia plain (Central Italy) combining PSI and GNSS data. *Remote Sensing*, *10*(7), 1146. https://doi.org/10.3390/rs10071146

Dinerstein, E., Olson, D., Joshi, A., Vynne, C., Burgess, N. D., Wikramanayake, E., et al. (2017). An ecoregion-based approach to protecting half the terrestrial realm. *BioScience*, *67*(6), 534–545. https://doi.org/10.1093/biosci/bix014

Dong, S., Samsonov, S., Yin, H., Ye, S., & Cao, Y. (2014). Time-series analysis of subsidence associated with rapid urbanization in Shanghai, China measured with SBAS InSAR method. *Environmental Earth Sciences*, *72*(3), 677–691. https://doi.org/10.1007/s12665-013-2990-y

Du, Y., Feng, G., Liu, L., Fu, H., Peng, X., & Wen, D. (2020). Understanding land subsidence along the coastal areas of Guangdong, China, by analyzing multi-track MTInSAR data. *Remote Sensing*, *12*(2), 299. https://doi.org/10.3390/rs12020299

Ebrahimy, H., Feizizadeh, B., Salmani, S., & Azadi, H. (2020). A comparative study of land subsidence susceptibility mapping of Tasuj plane, Iran, using boosted regression tree, random forest and classification and regression tree methods. *Environmental Earth Sciences*, *79*(10), 223. https://doi.org/10.1007/s12665-020-08953-0

El Kamali, M., Papoutsis, I., Loupasakis, C., Abuelgasim, A., Omari, K., & Kontoes, C. (2021). Monitoring of land surface subsidence using persistent scatterer interferometry techniques and ground truth data in arid and semi-arid regions, the case of Remah, UAE. *Science of the Total Environment*, *776*. https://doi.org/10.1016/j.scitotenv.2021.145946

Ellis, E. C., & Ramankutty, N. (2008). Putting people in the map: Anthropogenic biomes of the world. *Frontiers in Ecology and the Environment*, *6*(8), 439–447. https://doi.org/10.1890/070062

Erban, L. E., Gorelick, S. M., & Zebker, H. A. (2014). Groundwater extraction, land subsidence, and sea-level rise in the Mekong Delta, Vietnam. *Environmental Research Letters*, *9*(8), 084010. https://doi.org/10.1088/1748-9326/9/8/084010

Fick, S. E., & Hijmans, R. J. (2017). WorldClim 2: New 1-km spatial resolution climate surfaces for global land areas. *International Journal of Climatology*, *37*(12), 4302–4315. https://doi.org/10.1002/joc.5086

Gao, J. (2020). Global 1-km downscaled population base year and projection grids based on the shared socioeconomic pathways, Revision 01. https://doi.org/10.7927/q7z9-9r69

Gebremichael, E., Sultan, M., Becker, R., El Bastawesy, M., Cherif, O., & Emil, M. (2018). Assessing land deformation and sea encroachment in the Nile Delta: A radar interferometric and inundation modeling approach. *Journal of Geophysical Research: Solid Earth*, *123*(4), 3208–3224. https://doi.org/10.1002/2017JB015084

Haghshenas Haghighi, M., & Motagh, M. (2019). Ground surface response to continuous compaction of aquifer system in Tehran, Iran: Results from a long-term multi-sensor InSAR analysis. *Remote Sensing of Environment*, *221*, 534–550. https://doi.org/10.1016/j.rse.2018.11.003

Hartmann, J., & Moosdorf, N. (2012). The new global lithological map database GLiM: A representation of rock properties at the Earth surface. *Geochemistry, Geophysics, Geosystems*, *13*(12), Q12004. https://doi.org/10.1029/2012GC004370

Heleno, S. I. N., Oliveira, L. G. S., Henriques, M. J., Falcão, A. P., Lima, J. N. P., Cooksley, G., et al. (2011). Persistent Scatterers Interferometry detects and measures ground subsidence in Lisbon. *Remote Sensing of Environment*, *115*(8), 2152–2167. https://doi.org/10.1016/j.rse.2011.04.021

Hengl, T., De Jesus, J. M., Heuvelink, G. B. M., Gonzalez, M. R., Kilibarda, M., Blagotić, A., et al. (2017). SoilGrids250m: Global gridded soil information based on machine learning. *PLoS One*, *12*(2), e0169748. https://doi.org/10.1371/journal.pone.0169748

Heywood, C. E., Galloway, D. L., & Stork, S. V. (2002). *Ground displacements caused by aquifer- system water-level variations observed using interferometric synthetic aperture radar near Albuquerque, New Mexico ground displacements caused by aquifer- system water-level variations observed using interferometri*. U.S. Geological Survey Water-Resources Water-Resources Investigations Report 02-4235.

Ho Tong Minh, D., Van Trung, L., & Le Toan, T. (2015). Mapping ground subsidence phenomena in Ho Chi Minh City through the radar interferometry technique using ALOS PALSAR data. *Remote Sensing*, *7*(7), 8543–8562. https://doi.org/10.3390/rs70708543

Hwang, C., Yang, Y., Kao, R., Han, J., Shum, C. K., Galloway, D. L., et al. (2016). Time-varying land subsidence detected by radar altimetry: California, Taiwan and North China. *Scientific Reports*, *6*(1), 28160. https://doi.org/10.1038/srep28160

Joint Research Centre. (n.d.). Global land cover 2000 (2003). Retrieved from https://forobs.jrc.ec.europa.eu/products/glc2000/glc2000.php

Kakar, N., Kakar, D. M., & Barrech, S. (2020). Land subsidence caused by groundwater exploitation in Quetta and surrounding region, Pakistan. *Proceedings of the International Association of Hydrological Sciences*, *382*, 595–607. https://doi.org/10.5194/piahs-382-595-2020

Khorrami, M., Abrishami, S., Maghsoudi, Y., Alizadeh, B., & Perissin, D. (2020). Extreme subsidence in a populated city (Mashhad) detected by PSInSAR considering groundwater withdrawal and geotechnical properties. *Scientific Reports*, *10*(1), 11357. https://doi.org/10.1038/s41598-020-67989-1

Kottek, M., Grieser, J., Beck, C., Rudolf, B., & Rubel, F. (2006). World map of the Köppen-Geiger climate classification updated. *Meteorologische Zeitschrift*, *15*(3), 259–263. https://doi.org/10.1127/0941-2948/2006/0130

Li, J., Wang, S., Michel, C., & Russell, H. A. J. (2020). Surface deformation observed by InSAR shows connections with water storage change in Southern Ontario. *Journal of Hydrology: Regional Studies*, *27*, 100661. https://doi.org/10.1016/j.ejrh.2019.100661

Li, X., Yan, L., Lu, L., Huang, G., Zhao, Z., & Lu, Z. (2021). Adjacent-track InSAR processing for large-scale land subsidence monitoring in the Hebei Plain. *Remote Sensing*, *13*(4), 1–23. https://doi.org/10.3390/rs13040795

Malik, K., Kumar, D., Perissin, D., & Pradhan, B. (2022). Estimation of ground subsidence of New Delhi, India using PS-InSAR technique and multi-sensor Radar data. *Advances in Space Research*, *69*(4), 1863–1882. https://doi.org/10.1016/j.asr.2021.08.032

Marthews, T. R., Dadson, S. J., Lehner, B., Abele, S., & Gedney, N. (2015). High-resolution global topographic index values for use in large-scale hydrological modelling. *Hydrology and Earth System Sciences*, *19*(1), 91–104. https://doi.org/10.5194/hess-19-91-2015

Mekonnen, M. M., & Hoekstra, A. Y. (2011). National water footprint accounts: The green, blue and grey water footprint of production and consumption, value of water research report series No. 50. *Hydrology and Earth System Sciences Discussions*, *8*.

Motagh, M., Shamshiri, R., Haghshenas Haghighi, M., Wetzel, H. U., Akbari, B., Nahavandchi, H., et al. (2017). Quantifying groundwater exploitation induced subsidence in the Rafsanjan plain, southeastern Iran, using InSAR time-series and in situ measurements. *Engineering Geology*, *218*, 134–151. https://doi.org/10.1016/j.enggeo.2017.01.011

Najafi, Z., Pourghasemi, H. R., Ghanbarian, G., & Fallah Shamsi, S. R. (2020). Land-subsidence susceptibility zonation using remote sensing, GIS, and probability models in a Google Earth Engine platform. *Environmental Earth Sciences*, *79*(21), 491. https://doi.org/10.1007/s12665-020-09238-2

Ng, A. H. M., Ge, L., Li, X., Abidin, H. Z., Andreas, H., & Zhang, K. (2012). Mapping land subsidence in Jakarta, Indonesia using persistent scatterer interferometry (PSI) technique with ALOS PALSAR. *International Journal of Applied Earth Observation and Geoinformation*, *18*(1), 232–242. https://doi.org/10.1016/j.jag.2012.01.018

Othman, A., & Abotalib, A. Z. (2019). Land subsidence triggered by groundwater withdrawal under hyper-arid conditions: Case study from Central Saudi Arabia. *Environmental Earth Sciences*, *78*(7), 243. https://doi.org/10.1007/s12665-019-8254-8

Othman, A., Sultan, M., Becker, R., Alsefry, S., Alharbi, T., Gebremichael, E., et al. (2018). Use of geophysical and remote sensing data for assessment of aquifer depletion and related land deformation. *Surveys in Geophysics*, *39*(3), 543–566. https://doi.org/10.1007/s10712-017-9458-7

Pagani, M., Garcia-Pelaez, J., Gee, R., Johnson, K., Poggi, V., Styron, R., et al., (2018). Global earthquake model global seismic hazard (p. 475).

Parker, A. L., Filmer, M. S., & Featherstone, W. E. (2017). First results from sentinel-1A InSAR over Australia: Application to the Perth Basin. *Remote Sensing*, *9*(3), 299. https://doi.org/10.3390/rs9030299

Pelletier, J. D., Broxton, P. D., Hazenberg, P., Zeng, X., Troch, P. A., Niu, G. Y., et al. (2016). A gridded global data set of soil, intact regolith, and sedimentary deposit thicknesses for regional and global land surface modeling. *Journal of Advances in Modeling Earth Systems*, *8*(1), 41–65. https://doi.org/10.1002/2015MS000526

Pourghasemi, H. R., & Mohseni Saravi, M. (2019). Land-subsidence spatial modeling using the random forest data-mining technique. In *Spatial modeling in GIS and R for Earth and environmental sciences* (pp. 147–159). https://doi.org/10.1016/b978-0-12-815226-3.00006-5

Rafiei Sardooi, E., Pourghasemi, H. R., Azareh, A., Soleimani Sardoo, F., & Clague, J. J. (2021). Comparison of statistical and machine learning approaches in land subsidence modelling. *Geocarto International*, *37*(21), 6165–6185. https://doi.org/10.1080/10106049.2021.1933211

Raspini, F., Cigna, F., & Moretti, S. (2012). Multi-temporal mapping of land subsidence at basin scale exploiting persistent scatterer interferometry: Case study of Gioia Tauro plain (Italy). *Journal of Maps*, *8*(4), 514–524. https://doi.org/10.1080/17445647.2012.743440

Raspini, F., Loupasakis, C., Rozos, D., & Moretti, S. (2013). Advanced interpretation of land subsidence by validating multi-interferometric SAR data: The case study of the Anthemountas basin (Northern Greece). *Natural Hazards and Earth System Sciences*, *13*(10), 2425–2440. https://doi.org/10.5194/nhess-13-2425-2013

Rohatgi, A. (n.d.). WebPlotDigitizer. Retrieved from https://automeris.io/WebPlotDigitizer

Salehi Moteahd, F., Hafezi Moghaddas, N., Lashkaripour, G. R., & Dehghani, M. (2019). Geological parameters affected land subsidence in Mashhad plain, north-east of Iran. *Environmental Earth Sciences*, *78*(14), 405. https://doi.org/10.1007/s12665-019-8413-y

Sekkeravani, M. A., Bazrafshan, O., Pourghasemi, H. R., & Holisaz, A. (2022). Spatial modeling of land subsidence using machine learning models and statistical methods. *Environmental Science and Pollution Research*, *29*(19), 28866–28883. https://doi.org/10.1007/s11356-021-18037-6

Subsidence in San Joaquin Valley. (n.d.). Subsidence in San Joaquin valley. Retrieved from https://mavensnotebook.com/2013/11/22/in-her-own-words-usgs-hydrologist-discusses-subsidence-in-the-central-valley/

Sutanudjaja, E. H., Van Beek, R., Wanders, N., Wada, Y., Bosmans, J. H. C., Drost, N., et al. (2018). PCR-GLOBWB 2: A 5 arcmin global hydrological and water resources model. *Geoscientific Model Development*, *11*(6), 2429–2453. https://doi.org/10.5194/gmd-11-2429-2018

TRE Altamira Dataset. (2015). Retrieved from https://data.cnra.ca.gov/dataset/tre-altamira-insar-subsidence/resource/2535a9b9-ed25-4b19-9734-4b1409e3fdce

USGS. (1996). GTOPO30: Global 30 arc second elevation data set. Retrieved from https://www1.Gsi.Go.Jp/Geowww/Globalmap-Gsi/Gtopo30/Gtopo30.Html

van der Horst, T., Rutten, M. M., van de Giesen, N. C., & Hanssen, R. F. (2018). Monitoring land subsidence in Yangon, Myanmar using Sentinel-1 persistent scatterer interferometry and assessment of driving mechanisms. *Remote Sensing of Environment*, *217*, 101–110. https://doi.org/10.1016/j.rse.2018.08.004

Wen, T., Tiewang, W., Arabameri, A., Asadi Nalivan, O., Pal, S. C., Saha, A., & Costache, R. (2022). Land-subsidence susceptibility mapping: Assessment of an adaptive neuro-fuzzy inference system–genetic algorithm hybrid model. *Geocarto International*, *37*(26), 12194–12218. https://doi.org/10.1080/10106049.2022.2066198

World Administrative Boundaries. (n.d.). World administrative boundaries. Retrieved from https://public.opendatasoft.com/explore/dataset/world-administrative-boundaries/export/?dataChart=eyJxdWVyaWVzIjpbeyJjb25maWciOnsiZGF0YXNldCI6Indvcmxk LWFkbWluaXN0cmF0aXZlLWJvdW5kYXJpZXMiLCJvcHRpb25zIjp7fX0sImNoYXJ0cyI6W3siYWxpZ25Nb250aCI6dHJ1ZSwidHlwZSI6I

Yu, J., Wang, G., Kearns, T. J., & Yang, L. (2014). Is there deep-seated subsidence in the Houston-Galveston area? *International Journal of Geophysics*, *2014*, 1–11. https://doi.org/10.1155/2014/942834

Zamanirad, M., Sarraf, A., Sedghi, H., Saremi, A., & Rezaee, P. (2020). Modeling the influence of groundwater exploitation on land subsidence susceptibility using machine learning algorithms. *Natural Resources Research*, *29*(2), 1127–1141. https://doi.org/10.1007/s11053-019-09490-9